Three-Dimensional Characterization of Microstructure by Electron Back-Scatter Diffraction

Anthony D. Rollett,[1] S.-B. Lee,[1] R. Campman,[2] and G.S. Rohrer[1]

[1]Materials Science and Engineering Department, Carnegie Mellon University, Pittsburgh, Pennsylvania 15213; email: rollett@andrew.cmu.edu

[2]United States Steel Corporation, Clairton Works, Clairton, Pennsylvania 15025

Key Words

orientation scanning, statistical reconstruction, microscopy, texture

Abstract

The characterization of microstructures in three dimensions is reviewed, with an emphasis on the use of automated electron back-scatter diffraction techniques. Both statistical reconstruction of polycrystalline structures from multiple cross sections and reconstruction from parallel, serial sections are discussed. In addition, statistical reconstruction of second-phase particle microstructures from multiple cross sections is reviewed.

Report Documentation Page		

1. REPORT DATE **2007**	2. REPORT TYPE	3. DATES COVERED **00-00-2007 to 00-00-2007**

4. TITLE AND SUBTITLE **Three-Dimensional Characterization of Microstructure by Electron Back-Scatter Diffraction**	5a. CONTRACT NUMBER
	5b. GRANT NUMBER
	5c. PROGRAM ELEMENT NUMBER
6. AUTHOR(S)	5d. PROJECT NUMBER
	5e. TASK NUMBER
	5f. WORK UNIT NUMBER
7. PERFORMING ORGANIZATION NAME(S) AND ADDRESS(ES) **Carnegie Mellon University,Department of Material Science and Engineering ,5000 Forbes Avenue,Pittsburgh,PA,15213**	8. PERFORMING ORGANIZATION REPORT NUMBER
9. SPONSORING/MONITORING AGENCY NAME(S) AND ADDRESS(ES)	10. SPONSOR/MONITOR'S ACRONYM(S)
	11. SPONSOR/MONITOR'S REPORT NUMBER(S)

12. DISTRIBUTION/AVAILABILITY STATEMENT
Approved for public release; distribution unlimited

13. SUPPLEMENTARY NOTES

14. ABSTRACT
see report

15. SUBJECT TERMS

16. SECURITY CLASSIFICATION OF:			17. LIMITATION OF ABSTRACT **Same as Report (SAR)**	18. NUMBER OF PAGES **32**	19a. NAME OF RESPONSIBLE PERSON
a. REPORT **unclassified**	b. ABSTRACT **unclassified**	c. THIS PAGE **unclassified**			

MOTIVATION

We review briefly the motivation for the characterization of materials in three dimensions. Most materials of practical value are polycrystalline, and the arrangement of the crystals or grains in space is usually sufficiently complicated that plane sections do not suffice to describe microstructure quantitatively. Furthermore, most properties, even in materials with cubic crystal symmetry, are anisotropic, which means that even small deviations from uniform (random) texture lead to anisotropic behavior of the polycrystal. Elastic response is mildly anisotropic in most cases, and the plastic response of a material can be strongly anisotropic. A further complication is that many processing routes lead to heterogeneous microstructures, so it is often necessary to characterize the gradients in microstructure and accept that there is not a single representative microstructure. Although it is an accepted axiom of materials science that properties depend on microstructure, it is worth pointing out the great variety of important problems that are known to be sensitive to microstructure, such as surface roughening, intergranular corrosion, fatigue crack initiation and initiation, fracture toughness, hot ductility dip cracking, electromigration, and hillock formation.

In surface roughening, for example, three-dimensional characterization is important because the grains beneath the surface layer may affect the development of variable surface height as strain increases (1). Intergranular corrosion in its more serious manifestations leads to extensive penetration of the chemical reactions along grain boundaries. Such attack is necessarily three dimensional in nature, and so it is self-evident that comparisons of predictions of vulnerability with grain boundary character require three-dimensional characterization. The fundamentals of fatigue crack initiation have been studied predominantly in pure single-phase metals and relatively little in engineering alloys. Nevertheless, in many real-life situations, a substantial fraction of the useful fatigue life is associated with the crack initiation phase. Cracks often develop from local variations in composition or structure such as constituent particles in aluminum alloys (2). They then grow in a seemingly irregular manner, which is presumed to be crystallographic, although quantitative evidence is lacking as yet. Again, three-dimensional characterization will self-evidently be needed in this case.

SCOPE OF PAPER

This paper attempts to review the current state of knowledge on the characterization of microstructures using automated electron back-scatter diffraction (EBSD), also known as orientation imaging microscopy (OIM^{TM}). EBSD is assumed to be a sufficiently familiar technique about which readers can consult appropriate reviews as needed (3, 4). Instead, this paper focuses on the use of EBSD to characterize three-dimensional materials. The method provides very complete information on lattice orientation, which permits many aspects of microstructure to be addressed. In addition to purely EBSD-based approaches, mention is also made of three-dimensional characterization that employs other sources of data, such as synchrotron radiation and optical microscopy for particle characterization.

The major sections of the review are as follows: implications of three-dimensional characterization, issues that arise in performing such characterization, possible technical approaches, statistical reconstruction of three-dimensional microstructures, reconstruction from serial sections, statistical reconstruction of distributions of second-phase particles, the use of synchrotron radiation for (complete) three-dimensional microstructures, and remaining challenges in three-dimensional characterization. Our view is that modern materials characterization goes far beyond the traditional provision of micrographs exhibiting typical microstructures with qualitative interpretation and, possibly, a measurement of grain size. Instead, the materials scientist must expect to be responsible for providing three-dimensional digital microstructures that are representative of a given material and that provide quantitative information on the distribution of structural parameters.

IMPLICATIONS

The characterization of materials should always be performed with a goal in mind. The reason for needing a goal is that characterization, especially in three dimensions, is expensive. Most materials have complex microstructures, and it is infeasible to measure all possible microstructural features. Even if the focus is on a particular feature such as second-phase particles, the segment of the population that one attempts to measure depends on the motivating problem. For example, strength depends mainly on the mean obstacle spacing, which means that the population must be characterized to, say, +/− two standard deviations of the mean. If, in contrast, fatigue crack initiation is of interest, then one measures the upper tail of the distribution. The second example implies larger areas or volumes but lower resolution images as compared with the first.

The second, related issue is that of the representative volume element. Certain types of problems require instantiation of a material's digital representation for a simulation of annealing or deformation. Again, the choice of problem governs the size of the volume to be instantiated. A simple example is that of plastic strength of a polycrystal for which the orientation of each crystal relative to the principal stress directions affects the effective yield stress. In this case, the representation of the variability of orientation in a polycrystal requires several thousand independent orientations (and therefore grains) to be included in the model. Matthies & Wagner (5) have discussed the issue of how many individual orientations are required to represent a given texture to a specified accuracy. In contrast, the interaction between a particle and a surrounding grain is dominated by local behavior, and the volume can be limited to a single grain or perhaps a single shell of nearest-neighbor grains.

Implicit in these discussions is the choice of microstructural element. Plasticity problems generally focus on the grain structure, and so the statistics of interest are likely to be size and crystal orientation. The distributions of these quantities are both three-dimensional, with morphological orientation adding another two dimensions. Note that "size" assumes that a simple, regular shape such as an ellipsoid or a cuboid provides an acceptable representation of grain shape. Less regular shapes obviously require more complex descriptions possibly involving spectral analysis. Methods such

as Fourier transforms, generalized spherical harmonics, and kernel particle analysis have been developed for such needs (6; M.D. Uchic, M.D. Graef, R. Wheeler, & D.M. Dimiduk, unpublished data).

ISSUES

The basic internal structural units, the grains, are not uniform in size but exhibit distributions in shape, size, and orientation. Aspect ratios can vary enormously from nearly spherical to nearly laminate. The reason for these inconvenient features is processing history. Choice of particle source for compaction, particle consolidation, solidification practice, rolling, extrusion, recrystallization, and grain growth all involve deformation or coarsening, which in turn leads to these distributions. That grains obviously must fill space, coupled with the distribution in size, means that they cannot have simple, regular shapes such as spheres, cubes, or ellipsoids. Of course, idealized microstructures have been generated with special geometrical forms such as cube octahedra to tackle certain problems, but even these do not lend themselves to representation of realistic distributions of shape and size (7).

An interesting exception to the generally pessimistic view of mathematical methods available to microstructural science lies in powder packing, which is not the main focus of this review, although it is of general interest and so is only briefly mentioned here. Torquato's group, for example, has developed extensive analysis on the topic of two-phase microstructures (8). A rich set of techniques for building microstructures and describing them in terms of radial distribution functions and correlation functions is available. Such an approach builds on earlier work by Corson (9–12), Adams et al. (13), Lee et al. (14), and many others.

Other types of composites are simpler to represent; laminated composites, for example, are possibly the simplest. Any composite with a monodisperse structural element (particles, layers, fibers) has less geometrical complexity than do polycrystals. Notwithstanding this apparently dismissive statement, there is considerable complexity involved in representing woven fiber composites. Such composites have a very wide range of applications from airplanes to body armor. The interleaving of fibers in three dimensions raises issues that are analogous to those in polycrystals: To what level of detail must one represent the composite? Is it necessary to describe the individual fibers, or is it sufficient to describe bundles of fibers? Again, this topic diverts us from the main focus of three-dimensional microstructures based on diffraction scanning, so no further detail is given.

This review makes numerous references to distributions. For quantities such as particle size, the distributions are simple to deal with. There has been extensive debate over the appropriate theoretical form to fit experimental measurements because few of the measured distributions conform to the standard normal distribution or bell curve, even when the data are transformed to the logarithm of the size measure (e.g., References 15–17). Crystal orientation, however, is not so simple to describe because of the inherently spherical nature of rotations in three dimensions. In effect, to describe the texture of a polycrystal in a statistical sense, one must develop a distribution over the group of general three-dimensional rotations, or SO(3). A great

variety of parameters can and have been used, although Euler angles, Rodrigues vectors, and (unit) quaternions have proven most useful.

Texture

Texture is a substantial topic, so we summarize the basic aspects here while providing references to the standard works (18–21). Texture means crystallographic preferred orientation in which one seeks to quantify the relationship between the crystal axes of grains in a polycrystal and reference frame, defined as a set of axes associated with the external shape of the polycrystalline body. Most often the term texture is used in conjunction with X-ray pole figures, which are the most efficient experimental means of quantifying the average texture of a (polycrystalline) material. Most fundamental is the understanding that crystallographic orientation requires specification of a rotation. This rotation is most often used as an axis transformation to express properties known in crystal axes into properties in the frame of the material. The second vital piece of information is that rotations can be expressed in a wide variety of mathematical and not-so-mathematical parameterizations, all of which have three independent parameters. The standard symbol for orientation is g, but other symbols are used, especially for the less-well-known but very useful Rodrigues-Frank vectors and quaternions.

Table 1 provides a summary of commonly used parameterizations of crystallographic orientation. The entries are ordered by familiarity to materials scientists. Specification of a plane and direction by Miller indices is most intuitive but requires translation for numerical work. Euler angles are common because of the convenience of using series expansion methods based on generalized spherical harmonics. Serious computational work, however, uses quaternions for speed and simplicity (22, 23). Axis-angle descriptions are the most intuitive description of grain boundaries because of the intimate connection to crystal geometry, and Rodrigues-Frank vectors have some very attractive features for both representation and certain types of computation. A few conversion formulae are given in **Table 1** to provide some clarification of the meaning of the parameters. There are formulae available in the standard texts to convert between any pair of representations (18, 19).

The next step in understanding and using texture is to become familiar with the characteristic preferred orientations of the particular material and processing history of interest. This is far too broad a subject for treatment here, and the reader is referred to Kocks et al. (19) and Randle & Engler (21) for detailed information and analysis.

We now introduce the concept of misorientation, Δg, or the difference in orientation between two crystals, to which the properties of boundaries can be related. Mathematically, the misorientation is obtained by combining one orientation with the inverse of the other:

$$\Delta g = g_2 \cdot g_1^{-1}. \qquad\qquad 1.$$

The choice of which of the two orientations should be the inverse rotation depends on the representation used and whether the misorientation is to be expressed in the reference frame or in the local, crystal frame (24). The most common approach by far

Table 1   Summary of parameterizations of texture and orientation

Name	Parameters	Conversion formulae

Texture component: specifies alignment of a plane normal with the third sample direction [e.g., normal direction (ND)] and a crystal direction with the first sample direction [e.g., rolling direction (RD)]. Each normal and direction is, in effect, a unit vector, and they must be perpendicular, yielding three independent parameters.	$(hkl)[uvw]$	$\mathbf{b} = \dfrac{(u, v, w)}{\sqrt{u^2 + v^2 + w^2}} \; // \, \mathbf{RD}$
		
		$\mathbf{n} = \dfrac{(h, k, l)}{\sqrt{h^2 + k^2 + l^2}} \; // \, \mathbf{ND}$

Euler angles: specify a triple of rotations (transformations) about the Z, X, and Z directions. Many variants of Euler angles are known.	$g = g(\phi_1, \Phi, \phi_2)$	$g_{ij} = \begin{pmatrix} \cos\varphi_1 \cos\varphi_2 - & \sin\varphi_1 \cos\varphi_2 + & \sin\varphi_2 \sin\Phi \\ \sin\varphi_1 \sin\varphi_2 \cos\Phi & \cos\varphi_1 \sin\varphi_2 \cos\Phi & \\ -\cos\varphi_1 \sin\varphi_2 - & -\sin\varphi_1 \sin\varphi_2 + & \cos\varphi_2 \sin\Phi \\ \sin\varphi_1 \cos\varphi_2 \cos\Phi & \cos\varphi_1 \cos\varphi_2 \cos\Phi & \\ \sin\varphi_1 \sin\Phi & -\cos\varphi_1 \sin\Phi & \cos\Phi \end{pmatrix}$
(Orthogonal) matrix: The coefficients of an axis transformation are defined by $a_{ij} = \hat{e}'_i \cdot \hat{e}_j$, where the e are the unit basis vectors in the primed and unprimed coordinate systems. All columns and rows are unit vectors that reduce the number of independent coefficients to three.	$g_{ij} = \begin{pmatrix} a_{11} & a_{12} & a_{13} \\ a_{21} & a_{22} & a_{23} \\ a_{31} & a_{32} & a_{33} \end{pmatrix}$	$\begin{array}{c} \qquad\quad Sample \\ g = Crystal \begin{pmatrix} b_1 & t_1 & n_1 \\ b_2 & t_2 & n_2 \\ b_3 & t_3 & n_3 \end{pmatrix} \end{array}$
Axis-angle: The rotation axis is specified by a unit vector, $\boldsymbol{n}$, and the rotation angle by θ. For grain boundaries, the rotation axis is often specified in crystallographic terms with a set of Miller indices.	$g = g(\theta, \boldsymbol{n})$	$g_{ij} = \delta_{ij} \cos\theta + n_i n_j (1 - \cos\theta) + \sum_{k=1,3} \varepsilon_{ijk} n_k \sin\theta$
Rodrigues-Frank vector: the rotation axis but scaled by the tangent of the semiangle. In this space, all rotations that share a common rotation axis lie on a straight line.	$\rho = (\rho_1, \rho_2, \rho_3)$ $= \tan(\theta/2)\boldsymbol{n}$	$\rho_1 = \tan\left(\dfrac{\Phi}{2}\right) \sin\left(\dfrac{\phi_1 - \phi_2}{2}\right) \Big/ \cos\left(\dfrac{\phi_1 + \phi_2}{2}\right)$ $\rho_2 = \tan\left(\dfrac{\Phi}{2}\right) \cos\left(\dfrac{\phi_1 - \phi_2}{2}\right) \Big/ \cos\left(\dfrac{\phi_1 + \phi_2}{2}\right)$ $\rho_3 = \tan\left(\dfrac{\phi_1 + \phi_2}{2}\right)$

(*Continued*)

Table 1   (*Continued*)

Name	Parameters	Conversion formulae
Quaternion: closely related to the Rodrigues-Frank vector. The n_i are the components. For rotations, the quaternion is always of unit length. The quaternions representing θ and $2\pi\text{-}\theta$ are the negative of each other but represent the same orientation (2-to-1 mapping).	$q = (q_1, q_2, q_3, q_4)$ $= (\sin(\theta/2)n_1,$ $\sin(\theta/2)n_2, \sin(\theta/2)n_3,$ $\cos(\theta/2))$	$q_1 = \sin\left(\dfrac{\Phi}{2}\right)\cos\left(\dfrac{\phi_1 - \phi_2}{2}\right)$ $q_2 = \sin\left(\dfrac{\Phi}{2}\right)\sin\left(\dfrac{\phi_1 - \phi_2}{2}\right)$ $q_3 = \cos\left(\dfrac{\Phi}{2}\right)\sin\left(\dfrac{\phi_1 + \phi_2}{2}\right)$ $q_4 = \cos\left(\dfrac{\Phi}{2}\right)\cos\left(\dfrac{\phi_1 + \phi_2}{2}\right)$

is to express misorientations in crystal coordinates because that is the physically more meaningful approach in almost all cases. If the orientations are expressed as matrices representing axis transformations, then the misorientation (in the crystal frame) is calculated with the same expression as above a substitution of the transpose of the second matrix for the inverse.

Finally, we can illustrate the complicated effect of crystal symmetry, which results in many physically equivalent descriptions of any misorientation because of the multiplicity of ways in which crystal axes can be labeled. The following expression summarizes the way in which the smallest possible rotation angle can be identified. The formula for determining the smallest misorientation angle, θ^*, is as follows, where the symmetry operators, O, are drawn from the set of n members of the (proper rotation) point group appropriate to the crystal symmetry:

$$\theta^* = \min\left\{\cos^{-1}\left(\frac{trace\left(O^{(i)}g_B g_A^{-1} O^{(j)}\right) - 1}{2}\right),\right.$$
$$\left.\cos^{-1}\left(\frac{trace\left(O^{(k)}g_A g_B^{-1} O^{(l)}\right) - 1}{2}\right)\right\}, \quad \{i, j, k, l = 1, n\} \qquad 2.$$

The order of the two orientations can be interchanged without affecting the meaning of the result, so for the $n = 24$ symmetry operators in $O(432)$, there are 1152 combinations that must be calculated to find the unique description of misorientation for grain boundaries in cubic materials. Inspection of this expression reveals that it can also be used to specify the misorientation in a unique way. In fact, one can choose specific symmetry operators in such a way as to always locate the misorientation axis in a particular asymmetric unit such as the standard stereographic triangle for cubic materials. Detailed discussions of the mathematics can be found in Morawiec's (20) book.

TECHNICAL APPROACHES

Just as the resolution used for imaging is dictated by the measurement objectives, so too is the choice of geometrical representation of microstructure. Is it acceptable,

for example, to use a building-block approach with cubes (for equiaxed grains) or bricks (for elongated grain shapes) (e.g., Reference 25)? Provided that the detailed grain shape does not significantly affect the result or the arrangement of nearest-neighbor grains, such geometries are simple to construct. It is also simple to populate with orientations, provided that only the orientation distribution is significant for the properties of the polycrystal.

If, however, we accept the necessity of a representation of the polycrystal microstructure with an accurate representation of grain shape and connectivity to other grains, then we have at least two possibilities:

1. a regular grid discretization of the three-dimensional volume [easier geometry, but less efficient and less compatible with finite element method (FEM) systems], and
2. vertex-edge-volume discretization of the three-dimensional volume (more complex geometry but more efficient and more compatible with meshing for FEM systems).

Then we must consider possible sources of information. At present, there are three obvious possibilities:

1. Direct measurement, such as three-dimensional X-ray (diffraction) microscopy, generates information on a regular grid.
2. Indirect measurement, such as serial sectioning, also generates information on a regular grid but only after a nontrivial stage of registration or alignment of the successive layers. This has been extensively researched in the biological community because of the importance to cellular structures. For reconstruction from serial sections of polycrystalline solids, it has been considered by a number of authors (26, 27) but is reexamined briefly here.
3. Statistical reconstruction based on limited cross-sectional information but on more than one sectioning plane; this is the main focus of this paper. Statistical methods for reconstructing microstructures have been developed in a number of fields (e.g., 28–35).

STATISTICAL RECONSTRUCTION: GRAIN-BASED

Grain Geometry

For a polycrystalline material, the critical feature is that of the grains. The generation of a representative digital microstructure therefore depends on obtaining a reasonable spatial arrangement of the grains along with their crystallographic orientations. Another critical feature is the requirement for statistical homogeneity of the material: it must be possible to generate cross sections in different locations of the material while characterizing what is, statistically, the same material. A choice is then required as to how to construct the geometry. The traditional approach for composites apparently has been to distribute the required volume fraction of second phase in the simulation domain and then to devise an algorithm to rearrange until sufficiently good agreement is obtained with some set of statistics obtained from experimental data (8). For an example of the recent application of genetic algorithms to this problem, see Basanta et al.

(36, 37). The issue that arises with polycrystalline microstructures, however, is the number of distinct structural units, i.e., grains, that must be manipulated to optimize a packing. That is, it is no longer sufficient to color the voxels black or white. Rather, one must number them according to the grain or orientation to which they belong. Each grain is reasonably compact in shape, which means that transferring individual voxels would result in either very long simulation times or fragmented grain structures. Therefore, it is sensible to use a more complex geometrical unit to represent a grain and seek an algorithm that optimizes the packing of the unit shape. The natural choice appears to be the ellipsoid because of its convenient mathematical properties.

Methods have been developed for packing ellipsoids [see work by Torquato (8) and Sastry and colleagues (38)]. In general, however, close packing of nonspherical objects is a difficult problem. Numerical methods are therefore used to compensate for lack of analytical approach. Because we want to fill space, which is slightly different from optimal packing (of incompressible objects) we allow for overlap as well as gaps. The objective function is written accordingly; variations in the functional form of the objective function remain largely unexplored, however. The method, referred to here as Microstructure Builder, starts with an overpacked structure and swaps ellipsoids in and out (mostly out) to achieve an optimal arrangement. The initialization has had some attention but only on an empirical basis. If a packing of grains is known, it is possible to fit an ellipsoid to each grain and use this ensemble of grains as an initial condition.

Microstructure Builder requires statistical data on the morphology of the grains in the polycrystal to be represented, which includes distributions of sizes and shapes. It also requires data on the texture (orientation distribution) and the grain boundary character (misorientation distribution). Although three-dimensional information is ideal, the method has been developed around two-dimensional cross-sectional data sources. A natural source of such information is that of EBSD maps (4, 18). At least two orthogonal planes of information are required, one perpendicular to the sample normal direction (ND) and the other perpendicular to the sample rolling direction (RD). Orthogonal planes are required to obtain information on the ellipsoid-shape distribution function. The ellipsoids used here are assumed to have their semiaxes aligned with the specimen axes although the method. Variable ellipsoid alignment would obviously be useful for certain microstructures, especially in those with elongated needle-shaped grains, which can be found in some nitrides. However, if the grain boundary character is not required to be fitted in the digital microstructure, a combination of conventional metallography (for grain shape) with texture measurement is sufficient.

Assuming that there is no gradient in grain size through the sample and that the ellipsoids have the same orientation, a homogeneous distribution of ellipsoids $f(a, b, c)$ is sufficient to represent the grain size and shape distribution. Even though the full form of $f(a, b, c)$ is impossible to calculate, one can approximate or estimate it by

$$f(a, b, c) = f(a, b) \cdot f(c \mid b). \qquad \qquad 3.$$

Both the joint probability distribution $f(a, b)$ and the conditional probabilty distribution $f(c \mid b)$ can be obtained from the set of orthogonal orientation scans. The

procedure to obtain these is described in detail elsewhere (39). The simulation domain is typically in the form of a cubical box whose dimensions are $1 \times 1 \times 1$, although in principle any rectangular form may be used. This box is populated with a sampling of ellipsoids drawn from the distribution $f(a, b, c)$. For this purpose, the distribution function $f(a, b, c)$ must be scaled appropriately. The values of the semiaxes a, b, and c must be expressed in terms of fractions of the box size, in this case 1. For each ellipsoid generated, the semiaxes are chosen from the given distribution function. This can be done through the generation of values for a', b', and c' such that $0 > a' \geq a_{max}$, $0 > b' \geq b_{max}$, and $0 > c' \geq c_{max}$, respectively. Next, a random number, say r_1, is generated. The choice of a', b', and c' is accepted if $f(a', b', c') \leq r_1$. If the choice is accepted, then the ellipsoid is placed inside the simulation box by random choosing of coordinates as its center. Thus, a set of overlapping ellipsoids is generated. The total number of ellipsoids generated is 10 to 100 times the target number of grains.

Packing of ellipsoids. Out of this set of ellipsoids, only a minimal subset is retained such that it optimally fills the simulation box. An optimal filling is defined as a system having minimal overlap and maximum space filling. This could be achieved by the solution of a many-body dynamics problem (see, for example, Reference 40). Because, as discussed above, there is no theory to indicate a unique solution to this problem, the approach discussed here uses Monte Carlo integration to approximate the packing.

A simulated annealing algorithm is used to choose a subset of the ellipsoids by minimizing the system energy. The algorithm proceeds in the following manner. A random subset of the ellipsoids is chosen from the original set such that the total volume contained in the subset is approximately the same as the box volume. The total energy of the system is evaluated whereby the energy is calculated in terms of overlap and gaps between the ellipsoids contained in the simulation domain (39). This energy is then minimized by a series of addition, subtraction, swap, and jog transactions. Any transaction that reduces the energy is accepted. If a transaction increases the energy, then it is accepted with a certain probability, depending on the amount of increase (which is a user input). The transactions allowed are addition, in which a randomly chosen ellipsoid is added to the existing set; subtraction, in which a randomly chosen ellipsoid is taken out of the set; swap, in which a randomly chosen ellipsoid in the set is replaced by another randomly chosen ellipsoid not in the set; and jog, in which a randomly chosen ellipsoid is replaced by another ellipsoid contained in it.

The procedure discussed above generates an optimal set of ellipsoids that forms the grain structure in the final microstructure. There may be regions within the simulation box that are contained in more than one ellipsoid and others that are not contained in any. The algorithm next invokes a Voronoi tessellation.

As discussed above, the requirement is to generate a nonoverlapping space-filling structure that provides volumes of individual grains and their grain boundary areas. This is accomplished by utilizing the properties of Voronoi diagram $V(P)$. The Voronoi diagram divides the space into Voronoi regions, which by definition is a nonoverlapping set. Computation of Voronoi diagrams can be carried out with the qvoronoi program (**http://www.qhull.org/**). To generate the Voronoi regions, the space is sampled randomly with a set of points S. For each of the sampled points in S,

the number of ellipsoids, from the set defined above, in which it is contained can be calculated. Out of these sampled points, only those contained in exactly one ellipsoid are retained. That is, if a point is contained by more than one ellipsoid or is contained in none, it is eliminated from *S*. Using this set *S*, we construct the Voronoi diagram *V(P)*. Brahme et al. (41) detail how this is implemented.

As the (Voronoi) cells themselves are nonoverlapping and space filling, the grains are just collections of cells, are also nonoverlapping, and are space filling. Also, because each grain is closely related to its enclosing ellipsoid, the grains have a similar shape and size distribution to that of the distribution function $f(a, b, c)$ that was used to generate the original set of ellipsoids. The detailed quantitative relationship between these distributions, however, has yet to be determined. The output microstructure obtained is in terms of Voronoi vertexes, edges, and patches. The volumes of each subset of Voronoi cells that represents a grain are obtained and used in the orientation assignment described below for calculating the orientation distribution. The areas between each pair of grains are also calculated and used in the orientation assignment for the calculation of the misorientation distribution, as discussed in the following section. **Figure 1** illustrates the result of generating a microstructure with 850 grains for a case in which strongly elongated grains were required to match a hot-rolled microstructure in a commercial purity aluminum alloy. The elongation was accomplished by applying a stretch (affine transformation) to a Voronoi tessellation that represented a nearly equiaxed structure and then sampling on a regular grid for subsequent modeling of recrystallization with a Monte Carlo model (41). The directions in the material are denoted by RD for rolling direction, which is the elongation direction; TD for transverse direction; and ND for normal direction, which is the compression direction. Equivalent designations are L for RD, T for TD, and S for ND, from which the cross sections perpendicular to the RD, TD, and ND are known as the ST, LS, and LT sections, respectively.
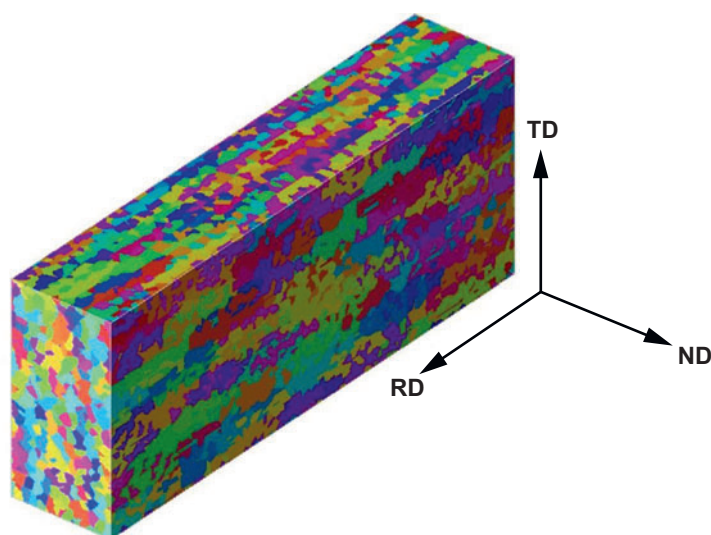

Figure 1

Three-dimensional digital microstructure obtained by statistical reconstruction for representation of a hot-rolled commercial purity aluminum alloy (41). ND, normal direction; RD, rolling direction; TD, transverse direction.

Grain Orientation

After establishing the geometry of the polycrystal, one can proceed to assign orientations to the grains. If only the texture affects the property to be calculated, then the objective function need only include the difference between the model orientation distribution (OD) and the measured OD. The current version starts with a random OD (but would be much more efficient with a sampled OD based on the measurements). The input OD is discretized in orientation space so that the OD of the digital microstructure can be compared, cell by cell, with the target (input) texture (42). One can also use a method based on a spherical harmonic expansion by calculating differences in values of the coefficients on the functions. If the property to be calculated also depends on the grain boundary character, then the misorientation distribution (MD) is also fitted. The current implementation also allows for the OD, $f(g)$, and MD, $f(\Delta g)$, to contribute (equal weight) to the objective function, S, as given below (39). Evolution of the fitted orientations is most conveniently performed with simulated annealing through the use of two types of change: swap of two orientations and change in a single orientation.

$$S = \sum_i (\text{OD}_{\text{fitted}}(g_i) - \text{OD}_{\text{measured}}(g_i)) - \sum_j (\text{MD}_{\text{fitted}}(\Delta g_j) - \text{MD}_{\text{measured}}(\Delta g_j)). \quad 4.$$

STATISTICAL RECONSTRUCTION: PARTICLE-BASED AT LOW VOLUME FRACTION

In this section, we discuss the statistical reconstruction of microstructures in which the key element is an ensemble of particles. In this case, orientations are not used because the dominant effect of particles is on processes such as fatigue and recrystallization in which the particles' size, location, and shape dominate the properties (but not crystal orientation). The primary characterization statistic is that of pair correlation functions (PCFs), i.e., correlation in position in each cross section, made on at least three different (orthogonal) section planes. In contrast to the problem of reconstructing grain structures in which the component grains must fit together to fill space, it is feasible to generate a separate reconstruction of the distribution of sizes, one that is independent of location. For particles that are monodisperse (in size, shape), this problem is well acknowledged and has semianalytical solutions for which the names Cahn and Saltykov are well known in the materials literature (43, 44); for a historical overview, see Underwood (45). Low volume fractions and noncontiguous particles are assumed (<10%) for what follows; however, the practicable upper limit of volume fraction has not been explored in this context. The most useful statistic for specifying particle locations so far has proved to be that of PCFs, which have been extensively developed by References 9, 39, and 46–50. An additional statistic that can be applied is that of ranked neighbor distances (51). This latter statistic places more emphasis on the nearby particles, whereas the PCF emphasizes medium to large particle spacings. Reconstruction of representative digital microstructures for two-phase materials has been discussed by several authors; see, for example, Rintoul & Torquato (52) and Singh et al. (53). These researchers have specifically addressed reconstruction of
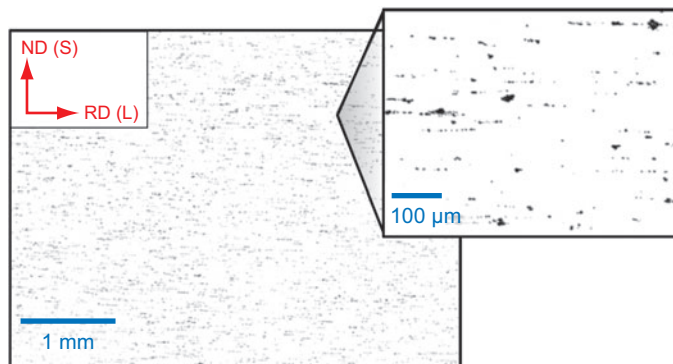
microstructures for discontinuously reinforced aluminum-based composites using
two-point correlation functions, which are closely related to the PCFs discussed
here.

The approach of reconstructing particle distributions based on PCFs is illustrated
with the case of an aerospace aluminum alloy. Samples were obtained from the bulk
of a two-inch-thick rolled AA7075 plate provided by the Alcoa Technical Center.
Details of the specimen preparation are given elsewhere (54). After all artifacts were
digitally removed, the images were binarized. The binarization of the images was
accomplished by the removal of small sections of the large image and the setting
of a threshold value for each section. Each binarized section was visually compared
with the original to determine the optimum threshold setting. After the optimum
threshold was achieved, the section was then placed back into the large stitched image.
Figures 2–4 present the large stitched images of each plane. The binarized images
were then converted to a pixel map format and analyzed. The algorithm locates each
particle center, calculates a PCF, and analyzes the size distribution of the particles.
To minimize the effects of noise, all particles smaller than two pixels are ignored, and
thus only particles with a diameter larger than 1.4 μm are included in the analysis.
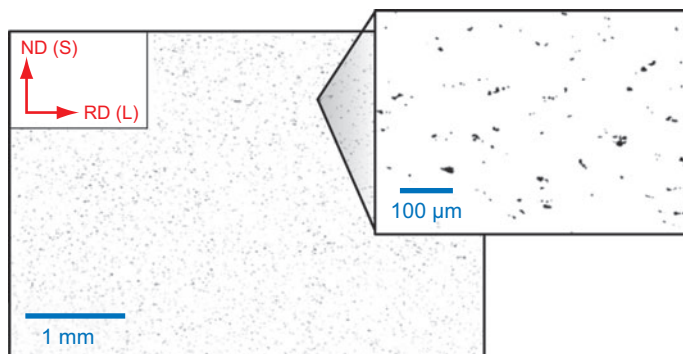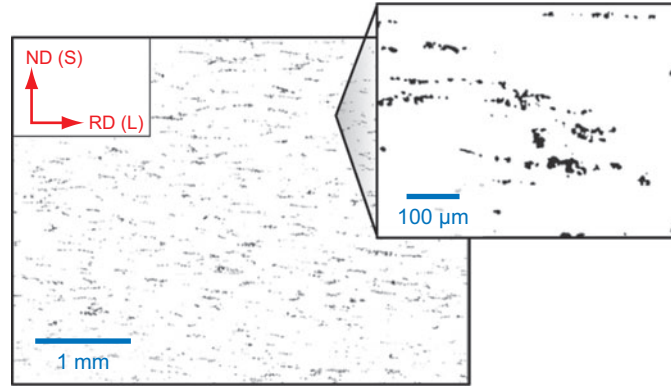
Figure 4

Image of constituent
particles in AA7075, L-T
plane.

Pair Correlation Functions

PCFs have been used in particle-stimulated nucleation of recrystallization studies to describe the placement of particles (48). The PCF is similar to the radial distribution function, which is used in solid-state physics (8). The radial distribution function gives the probability that a neighboring particle is located at a distance, r, in any direction in two dimensions.

The main difference between the PCF as used here and the radial distribution function is that the PCF is a function of both distance and angular orientation, whereas the radial distribution function is a function of only distance. In two dimensions, the PCF is a scalar function that defines the probability that a particle is located at the origin (0, 0) and that a different particle is located at coordinates (x, y). One can think of the PCF as the overlay of n copies of the image, one for each of n particles, where each copy is translated so as to place the center of each particle (in turn) at the center of the PCF; the intensity at each point in the PCF is then normalized by the number of particles and the area fraction of the image occupied by the particles. The PCF is calculated from a binarized image over a range of values for x and y according to

$$f(x, y) = \frac{1}{A_A} \sum_{i=1}^{n} \frac{P_i(x - a_i, y - b_i)}{\sum_i \Theta_i(x, y)}. \qquad 5.$$

Here n is the total number of particles, location (x, y) is referred to the origin of the PCF at (0, 0), P_i is the intensity in the image at the relative location $(x - a, y - b)$ for the ith particle at (a, b), and the sum in the denominator is the number of pixels that are within the boundaries of the image and contribute to the PCF at the location (x, y). The number of particles that contribute depends on how close the point is to the edge of the image.

Three-Dimensional Particle Structures

The incorporation of particles into a three-dimensional volume element is a four-step process that is accomplished with the aid of three programs written in C. Step one is
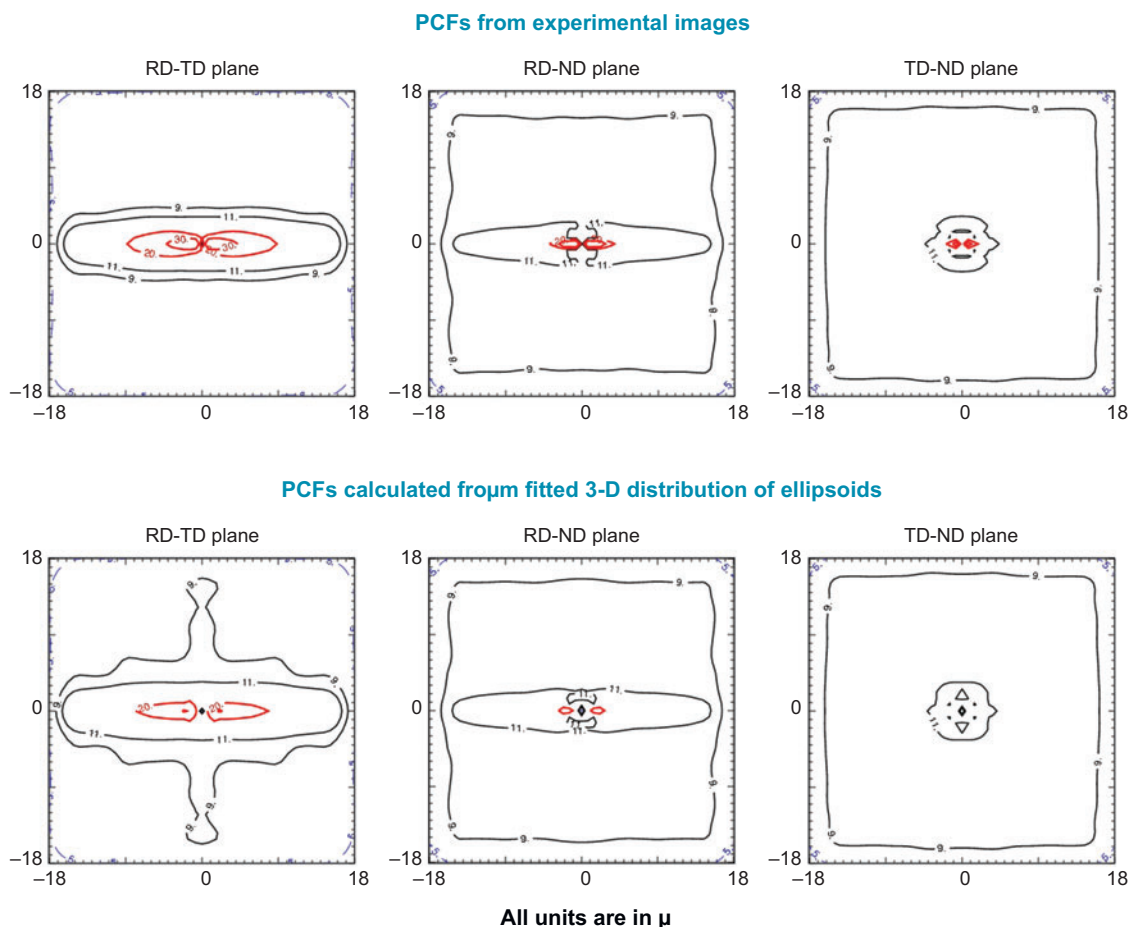
to calculate the PCFs of the particles from the binarized images. Step two is to create a set of ellipses that match the size and angular orientation of the particles in the two-dimensional image. An ellipse is created by first measuring a particle's moment of inertia. The ellipse's major and minor axes are then selected so that the moments of inertia of the ellipse match that of the particle. After three sets of ellipses have been generated from the three orthogonal planes, histograms containing their semimajor and semiminor axis lengths are created. In the third step, a set of ellipsoids is then created so that histograms of the semiaxis lengths of the sectioned ellipsoids (i.e., each ellipsoid becomes an ellipse on the section plane) match the histograms of the experimentally measured ellipses. This step is, in effect, a numerical implementation of the stereological problem of inferring a distribution of three-dimensional objects on the basis of cross-sectional information (45). The final step is to place the ellipsoids into the three-dimensional volume element by matching the PCFs measured from the three orthogonal two-dimensional images to cross sections taken from the three-dimensional volume element. **Figure 5** illustrates the results of developing a population of ellipsoids and placing within a volume element according to the measured PCFs. The resulting distribution of particles is illustrated in **Figure 6**, in which the stringering of the particles along the rolling direction is apparent.

At this stage of the development of the algorithms, EBSD is not a critical element in the development of three-dimensional models of low-volume-fraction particle populations such as the constituent particles in 7xxx series aluminum alloys illustrated in **Figure 4**. However, there is known to be a correlation between particle positions and grain boundaries (perhaps even triple lines) for which a combination of EBSD and particle imaging will be required. Roberts et al. (55) have quantified the correlation between particle position and interfaces in a Ni-base alloy as the particle-associated misorientation distribution function.

MICROSTRUCTURAL EVOLUTION: PARTICLE-BASED STRUCTURES AT HIGH VOLUME FRACTION

Although the packing method(s) described above can be applied to the case of two-phase systems at high volume fractions ($>50\%$), the result is unsatisfactory. One difficulty is that, at high volume fractions, the larger particles undergo soft impingement and are significantly distorted from regular ellipsoids. One way to address this type of digital microstructure is to use a model of the process by which the microstructure was generated. As an example, a recent effort generates representations of a W-Ni-Fe system, using simulation of the liquid-phase sintering that is typically employed to make this metal matrix composite.

A three-dimensional, Potts model of liquid-phase sintering (56) was developed on the basis of previous work in two dimensions (57, 58). The system of interest (W-Ni-Fe) exhibited full wetting of the solid. The kinetic Monte Carlo simulation method was used to probe coarsening dynamics and the characteristics of the solid particles, including the volume of critical nuclei and the distribution of particle size as a function of time. As expected for diffusion-limited coarsening, the average particle volume increases linearly with time. More importantly, the particle size distributions

PCFs from experimental images

PCFs calculated froµm fitted 3-D distribution of ellipsoids

All units are in µ

Figure 5

(*Upper row*) Pair correlation functions (PCFs) from experimental images for the RD-TD plane (rolling plane or LT section), RD-ND plane (longitudinal cross section or LS section), and TD-ND plane (transverse cross section or ST section). (*Lower row*) Corresponding PCFs calculated from the fitted three-dimensional distribution of ellipsoids. Contour levels have been multiplied by ten for easier viewing.

were nearly log-normal, which is consistent with those obtained experimentally, for example, in the W-Ni-Fe and Sn-Pb systems (59). In the obtaining of these results, careful consideration was given to the role of initial microstructural features in the subsequent evolution of the system. The resulting microstructures have been ported to a discretized fast-Fourier-transform model of plastic deformation for investigation of the dependence of the mechanical response to variations in microstructure such as contiguity between the W-rich particles. In this case, the use of EBSD is limited to maps that provide information on particle size and shape as well as on contiguity between particles that may be important to mechanical properties.
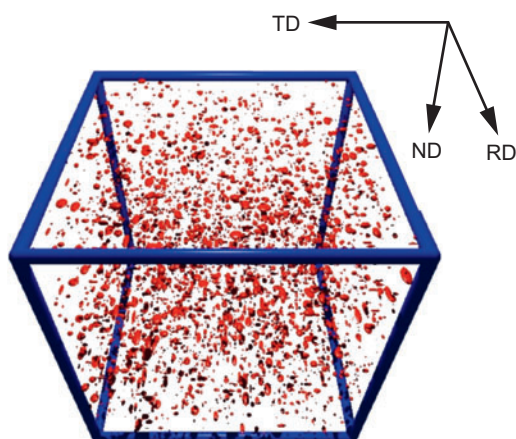
TD

ND   RD

STATISTICAL RECONSTRUCTION: LAYER-BASED FROM SERIAL SECTIONS

Registration of Adjacent Layers

The electron opacity of most crystalline materials provides a serious challenge to the complete characterization of the interfacial network. Full characterization of interfaces requires information about the inclination of the interfacial plane. Likewise, the full characterization of triple junctions requires the description of the orientation of the junction line itself. These data are inaccessible in a single-section characterization of the network. Three-dimensional reconstruction here refers to registry between the data upon any of the adjacent section planes obtained by calibrated (parallel) serial sectioning. Various papers relevant to the issues associated with polycrystalline solids (as opposed to the many articles in the biological literature) have been published on this problem (27, 60).

Two approaches have been taken in connection with the aforementioned analysis; these can also be combined. The first approach involves the use of external markers that are in common between any two adjacent section planes. A common example is the use of several hardness indentations that are observable on both planes. The centroid of the matching pairs of indentations on each plane can be used as the true and incorrect positions in Equation 6. The problem with external markers is associated with the fact that these markings are typically quite large relative to the features of interest in the microstructure. The determination of a precise location of the centroid of these features can be problematic, and thus errors can be large.

When precise registry between adjacent section planes is necessary, it is useful to employ internal markers. These are features of the microstructure itself that carry over from one section plane to the next. Examples include the orientations and phases of the grains themselves, the positions of triple junctions (as discussed below) and grain boundaries, twin boundaries, etc. Usually the use of internal markers requires one or more additional assumptions about the statistical nature of these markers' distribution in the microstructure. For example, it might be assumed that the orientation

distribution of the triple junctions is uniform (i.e., there is no preferred direction to the distribution of triple lines in the microstructure). The measured distribution can then be compared with the uniform model distribution (with its associated geometrical weighting factors) through Equation 5. In some instances (e.g., when twin boundaries are present in the microstructure), additional statistical assumptions may not be necessary.

The set of points $\{x_i\}$ associated with features in a specified two-dimensional planar section represents their reference positions, and the associated variable positions in the adjacent section plane are given by $\{y_i\}$. The relationship between reference and variable positions for any point is given by a combination of a rigid body rotation, R, and the translation vector, t, according to the expression

$$y = Rx + t. \qquad 6.$$

It is assumed that the component of the translation vector perpendicular to the section plane is a known constant. It is also typical to assume that an exact correspondence between the selected features common to both planes is known.

Generally, the coordinates of some number of features (e.g., boundaries, triple points, indentations) are measured in their reference and variable positions. It is then assumed that each point must be related in its reference and variable positions by the same (R, t) transformation. Thus,

$$y_i = Rx_i + t \quad (i = 1, 2, \ldots, N), \qquad 7.$$

where N is the number of feature points determined from the data. Experimental errors and the changes in feature locations from one section to the next mean that the relationships expressed in Equation 7 are only approximate, and a best fit for the transformation (R, t) must be obtained by the minimization of the objective function, ψ,

$$\psi = \sum_i \omega_i (y_i - (Rx_i + t))^2, \qquad 8.$$

where ω_i is a nonnegative weight assigned to the ith feature point.

An inherent physical assumption in the minimization problem expressed by Equation 8 exists: There is no directional anisotropy present in the set of feature points used in the analysis. For example, if common triple junctions are used as feature points, it is assumed that the triple junctions are randomly distributed in all directions. In cases in which this assumption is invalid, e.g., when materials have been subjected to (simple) shear deformations, any bias in the character of the distribution must be known to register the layers.

The minimization problem posed in Equation 8 has been widely applied for many years in various fields. A solution for the translation vector is given as the difference between the centroids of true and incorrect points according to the expression

$$t = \left(\sum_i \omega_i (y_i - Rx_i) \right) \bigg/ \sum_j \omega_j. \qquad 9.$$

The rotation R can be obtained from the polar decomposition of a certain matrix constructed from the x_i and y_i vectors (60). The method was applied to a small set

of two (nearly) parallel sections, each of which was identified to have 190 triple junctions. In this case, an affine transformation was allowed so that variable tilt and stretch between the two sections could be accommodated to optimize the alignment. The aligned sections were then used to extract true dihedral angles at all the triple junctions to calculate relative grain boundary energies (61).

Considerable experience has been gained with serial sectioning in recent years. Saylor et al. (62) have used serial sections to determine true dihedral angles in an MgO specimen, from which they determined grain boundary energies over the full five (macroscopic) degrees of freedom. The advent of techniques based around the focused ion beam has generated renewed interest because of the possibility of automating the sectioning while gathering orientation information on some or all of the section planes (63–77).

Example of Reconstruction from Serial Sections

Figure 7 shows examples of EBSD maps of two adjacent layers from a series of cross sections of a Ni-based alloy obtained through serial sectioning in a dual-beam system. For both panels of **Figure 7**, the black and speckled regions represent the collection of scanned pixels for which the EBSD system attempted to index a diffraction pattern but was not able to produce a solution. The central region with well-indexed points shows that a registration system based on orientation information must take into account the local quality of the data available. As illustrated in **Figure 7**, the position of the region of reliable data did not remain constant from layer to layer. For the TSL^{TM} system used in this instance, there are two indicators of quality, which are

Figure 7

Inverse pole figure maps of two adjacent sections of a Ni-based alloy. The thick red lines illustrate the edges of the area with reliable data (*left panel*). The abrupt deviation of the area of reliable data in the next layer (*right panel*) from the thick red lines indicates how each layer drifts laterally during the milling and EBSD mapping. The data were collected and provided by Air Force Research Laboratory (AFRL) via the FEI^{TM} system (73). The number of serial sections was 96, and the area of each scanned section was approximately 2,500 μm^2.

known as confidence index (CI) and image quality (IQ). The confidence index (CI) varies between −1 (poor) and 1 (good), and experience suggests that values above approximately 0.1 are reliable. Examination of the IQ values for this specific example suggested that poorly indexed pixels had IQ values below 100.

The registration was based on the assumption that the successive layers were sufficiently parallel that the only adjustment required was a translation limited to integer-valued shifts along x and y directions in each plane (i.e., the layers could be assumed to be parallel to one another, with no rotations between layers). In terms of Equations 6–9 above, this was equivalent to setting the rotation matrix, R, equal to the identity matrix but allowing the translation vector, t, to vary. In place of identifying specific microstructural features such as triple points, we used the orientation information inherent in the EBSD maps to align the successive layers, which exhibited significant displacements relative to one another (see **Figure 7**). The key assumption is that the separation between adjacent sections is smaller than the grain size; when this is true, each grain in a given section overlaps the corresponding grain in an adjacent section for a majority of its area. With the additional assumption that variations in orientation within a grain may be neglected, it is then reasonable to equate optimal registration with a minimum difference in orientation between pairs of pixels in the adjacent layers.

Accordingly, the objective function, ψ, was equated to the average disorientation $\langle D \rangle$ and calculated as shown in Equation 10 as the average of the disorientation, Δg, between each well-indexed pixel in the upper layer and its one or more neighboring pixels in the layer below, along with a weighting factor, ω, that decreases the contribution to $\langle D \rangle$ from points in the layer below having a low confidence index and low image quality. The expectation is that good alignment will generate a small average disorientation between pixels in adjacent layers.

$$\langle D(t) \rangle = \frac{1}{N} \sum_i \omega_i \Delta g_i(t), \quad \begin{cases} \omega_i = 1, & \text{if} \quad CI_{neigh} \geq 0.1 \quad \text{and} \quad IQ_{neigh} \geq 100 \\ \omega_i = (2.0 - 10.0 \times CI_{neigh}), & \text{otherwise} \end{cases}.$$

10.

Figure 8 illustrates the result of finding the minimum $\langle D(t) \rangle$ as a function of translation vector, t, for a particular pair of adjacent layers. The number of neighboring pixels contributing to the calculation of average disorientation was limited to one for this case, and the computation required a few minutes on a desktop computer. Notice that a sharp minimum exists in the average disorientation as a function of translations along the x and y directions, which identifies a particular translation, $t = (dx, dy)$, that can be used to register the two layers.

Three-Dimensional Microstructure from Serial Sections

Figure 9 illustrates the result of applying the above algorithm to the complete set of 96 layers of a Ni-based alloy. After registration, a cleanup procedure was applied: The grains smaller than 30 voxels in volume were absorbed into their neighbor grains. This cutoff size (30 voxels) was carefully chosen such that the grains eliminated were smaller than the smallest grains associated with the dominant size distribution. These
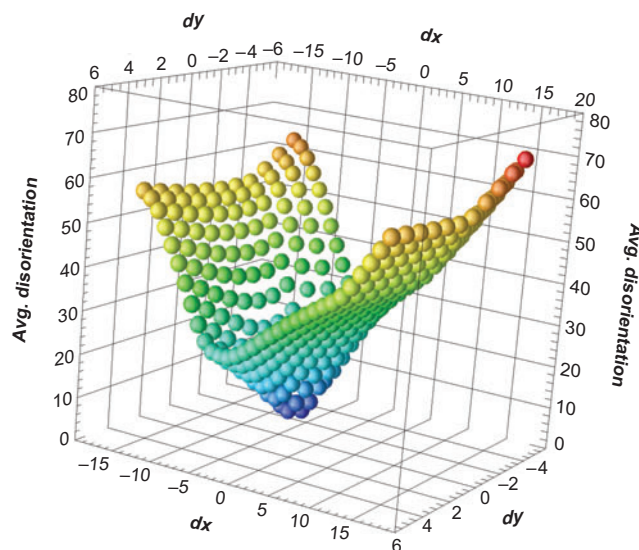
Average disorientation per pixel in a layer as a function of the translation in *x* and *y* directions of the layer below. The number of nearest-neighboring pixels included in the calculation of Equation 10 is one. The units of translation and average disorientation are pixels and degrees, respectively. For a particular alignment of the two layers, a well-defined minimum exists.

small "grains" were assumed to be either second-phase particles or poorly indexed points. Because of the relatively low stacking fault energy in this alloy, a high density of annealing twins was present in the material; these are evident as straight boundary traces in the sections. Most of the reconstructed annealing twins in the cross sections of the aligned structure also exhibited straight, flat sides, which suggests that the registration procedure was reasonably successful.
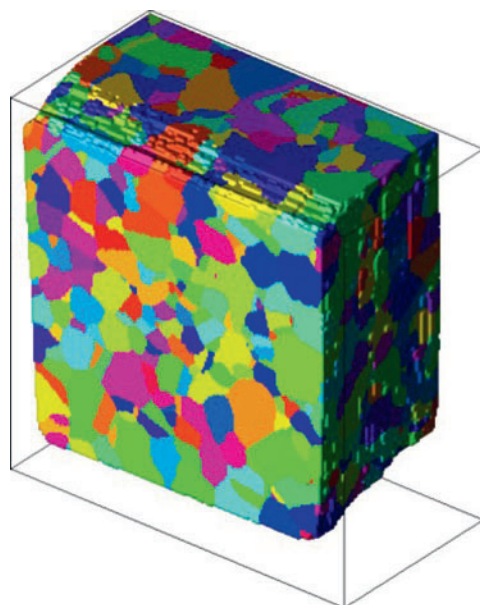

Figure 9
Aligned three-dimensional digital microstructure obtained by registering the layers with an objective function based on average disorientation between neighboring pixels in adjacent layers. In addition to performance of the registration, grains smaller than a specified cutoff value were removed from the structure.
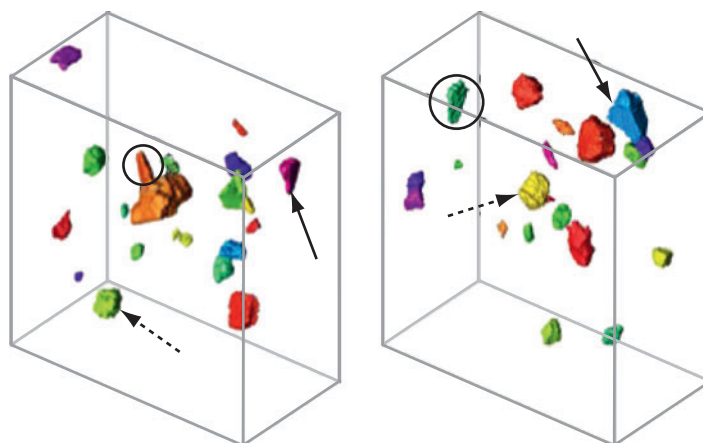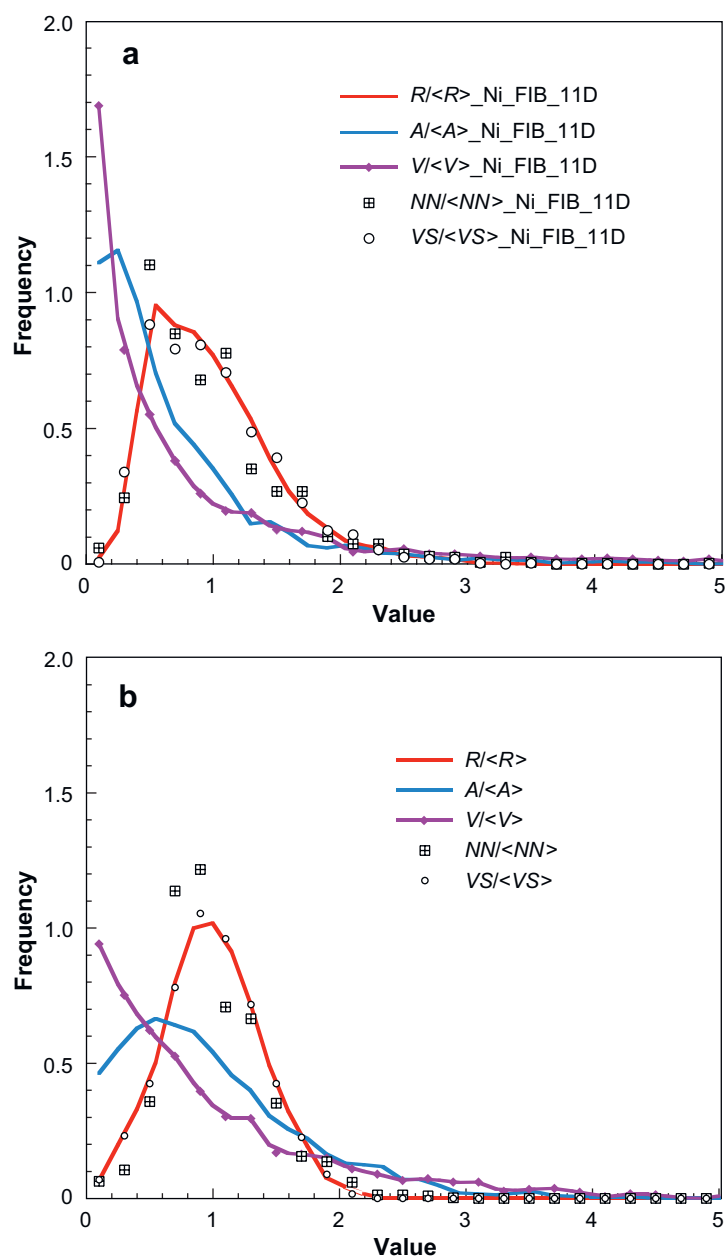
Figure 10

Morphologies of selected grains in the three-dimensional reconstructed microstructure. The individual grains were illustrated using different colors. The morphologies are equiaxed (marked with *dashed arrows*), plate-like annealing twins (marked with *circles*), or straight and flat sided (marked with *bold arrows*), suggesting that the alignment algorithm worked reasonably well.

Three-dimensional morphologies of the grains were examined by visualizing randomly selected grains to make sure that the proposed algorithm worked reasonably well. In **Figure 10**, the reconstructed microstructure contains a mix of equiaxed bulk grains; straight, flat-sided grains; and plate-like annealing twins. This again suggests that the alignment was successful.

STATISTICAL ANALYSIS OF THREE-DIMENSIONAL MICROSTRUCTURES

The aligned microstructure was analyzed for grain size distributions and for correlations between size and topology and also between size and volume:surface ratios. Grains that touch the exterior of the measured volume were excluded from the analysis, so 1325 out of a total of 1789 grains were measured. Distributions of the various measures of the microstructure provide a straightforward comparison to results in the literature. In **Figure 11a**, the distributions of radii, area, volume, nearest neighbors, and volume:surface ratio follow a similar pattern to that observed previously (78). Both the distributions of facets, F, and the volume:surface area ratios follow the radius distribution quite closely. **Figure 11b** shows the same statistics for a microstructure obtained from a Monte Carlo simulation of grain growth with isotropic properties on a periodic 130^3 grid and 1485 grains. The characteristics of the distributions are similar to those in the measured microstructure, with the following exception. The maximum reduced radius in the serial section data set lies above three, which is substantially larger than the cutoff at 2.1 in the simulation data set. Lastly, **Figure 11c** shows the same statistics for an equiaxed microstructure with 1490 grains, obtained from the statistical reconstruction process described above.

Figure 11

Plots of the distributions of normalized radius, area, volume, number of nearest neighbors (facets), and volume:surface ratio. Lines are drawn to guide the eye but do not represent specific functional forms. Both the number of neighbors and the volume:surface ratio follow a similar distribution to the radius. (*a*) Plot for the serial section data set of a Ni alloy. (*b*) Plot for a microstructure obtained from an isotropic grain growth model (80). The maximum reduced radius has a cutoff slightly above 2. (*c*) Plot based on a reconstruction from Microstructure Builder. The maximum reduced radius has a cutoff slightly above 2 and is approximately symmetrical about $R/\langle R \rangle = 1$.

The radius distribution is very nearly symmetrical about the mean size and has a narrower peak than that obtained with the measured microstructure or generated with the Monte Carlo simulation method. In all three cases, the distributions of number of nearest neighbors (facets) and the volume:size ratio follow the radius distribution quite closely.

Figure 11

(*Continued*)
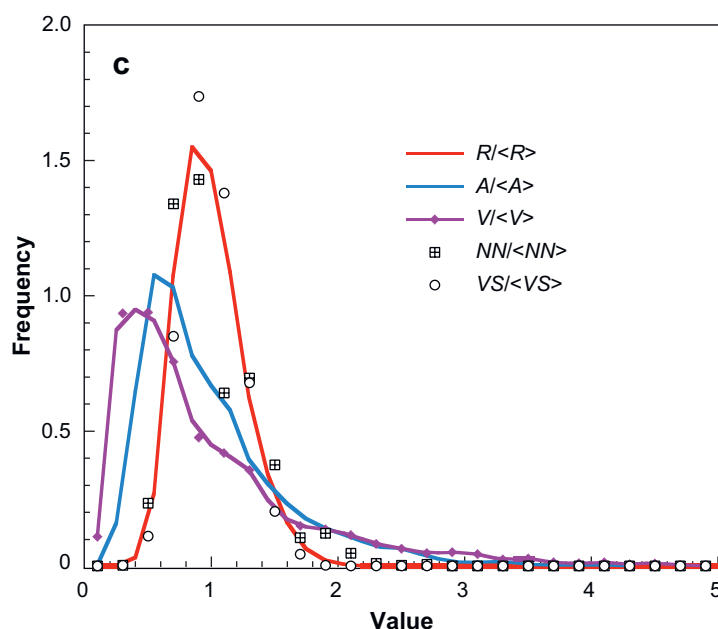
Examining the relationship between the size and number of nearest-neighbor grains (equal, obviously, to the number of facets) provides some insight into the relationship between linear dimension and the topological class. Here there are choices to be made about the measure of linear size; we adopt the sphere-equivalent radius as a simple measure of grain size, but many other possibilities, such as caliper diameter and mean width, exist (79). Another useful probe is the ratio of volume to surface area (*V/A*). This has dimensions of size, so the reasonable correlogram to plot is with (sphere-equivalent) radius because this reveals characteristics of shape. A sphere has a volume:surface ratio equal to 1/3, whereas, for example, a cube has a ratio of 1/6.

Figure 12 shows a plot of the number of nearest neighbors (also known as topological class) versus radius. As Liu et al. (78) note, it is possible to fit a straight line through the data, but a quadratic function results in a slightly better and more reasonable fit (with positive intercept on the vertical axis). For comparison with the Monte Carlo simulation microstructure and a microstructure generated with the ellipsoid packing algorithm described above, the respective data sets have been offset by 1 and 2 in the reduced radius.

The best fits to the data points for the Ni serial section, Monte Carlo, and Microstructure Builder data sets, respectively, are as follows:

$$F = 0.86 + 9.53 \, (R/\langle R \rangle) + 1.06 \, (R/\langle R \rangle)^2,$$
$$F = 3.29 + 5.96 \, (R/\langle R \rangle) + 3.45 \, (R/\langle R \rangle)^2,$$
$$F = 3.99 + 2.53 \, (R/\langle R \rangle) + 6.40 \, (R/\langle R \rangle)^2.$$

The coefficients demonstrate a steady trend from nearly linear for the experimental data set to more obviously quadratic for the Microstructure Builder data set.
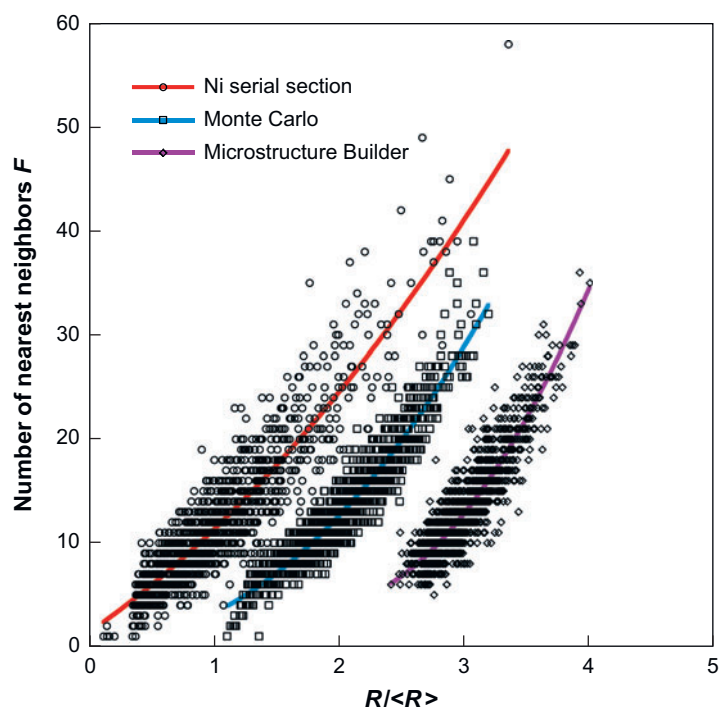
Plot of the number of nearest-neighbor grains (i.e., facets) against reduced radius for three different three-dimensional microstructures. The Monte Carlo and Microstructure Builder radius values are offset by 1 and 2, respectively, for clarity.

Another interesting statistic that should reveal grain shape is the ratio of volume to surface area (which has dimensions of length) divided by the (sphere-equivalent) diameter to obtain a dimensionless number. When this ratio is plotted against radius (**Figure 13**) for the three different microstructures, significant variations are apparent.

UNEXPLORED ISSUES

The alignment of serial exhibit a weaker texture than the largest grains, and as a consequence sections by exploiting orientation information in the layers as intrinsic markers is subject to the basic error that it cannot detect the existence of a shear strain in the microstructure. Although in principle extrinsic markers such as hardness indents are not subject to this vulnerability, in practice we suspect that a more secure check is orthogonal cross sections performed independently of the serial sectioning.

Spatial correlation of orientations is very commonly found in materials, particularly metallic alloys that have been subjected to extensive deformation by rolling, extrusion, or wire drawing. Although the phenomenon is commonplace, dealing with it in the reconstruction of three-dimensional microstructures is not necessarily straightforward. One might imagine that serial sectioning or direct imaging in the synchrotron would capture spatial correlation effects automatically. However, unless the correlation is studied in a quantitative fashion, there is no guarantee that the
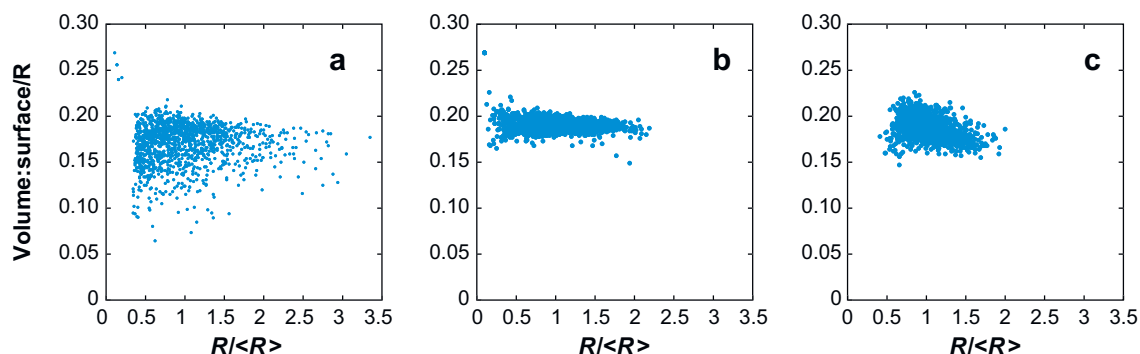
Figure 13

Plots of volume:surface area divided by (sphere-equivalent) radius, against reduced radius, for (*a*) the serial section data set; (*b*) the Monte Carlo data set, and (*c*) the Microstructure Builder data set. The experimental microstructure (*a*) exhibits the widest variation; the low values of volume:surface area may be associated with annealing twins. The Monte Carlo microstructure (*b*) shows a much narrower range of volume:surface ratio at the upper end (close to 0.2), suggesting more compact shapes than does the experimental structure. The Microstructure Builder (*c*) structure exhibits a wider range of volume:surface area ratio but over a narrower range of reduced radius.

volume sampled in serial sectioning will be large enough to provide a faithful representation of the material. For statistical reconstruction methods, the existence of spatial correlation means that a modified algorithm must be used for the assignment of orientations. One possible approach is to use two-point orientation functions, as Adams et al. (13) discuss. Such functions are computationally demanding, however, because of the size of the space required, and it may be more practical to use simplified measures of orientation coherence such as the disorientation correlation function as introduced by Lee et al. (81).

The correlation of orientation with grain size can also occur in materials as a result of microstructural evolution such as recrystallization. The group in Metz (82) has clearly documented such a correlation in hexagonal metals such as titanium and zirconium. In this example, the smallest grains the texture changes to that of the largest grains during subsequent grain growth. The same comments about the impact of orientation-location correlation discussed above apply to this type of correlation.

CONCLUSIONS

This review aims to convince the reader that three-dimensional characterization of materials via automated EBSD is feasible, albeit at an early stage of development. Digital microstructures, i.e., computer-based numerical descriptions, have been generated for a number of different materials and used as instantiations for calculations of properties in both polycrystalline materials and two-phase materials. Both statistically based reconstructions are feasible for polycrystals and composites. Furthermore, automated tools for serial sectioning using either metallographic techniques or ion beam

milling, combined with EBSD, have made it possible to perform three-dimensional characterization directly, albeit destructively.

SUMMARY POINTS

1. The topic of characterizing microstructures in three dimensions is discussed, with a particular emphasis on using the widely available technique of automated EBSD in the scanning electron microscope.

2. Two main approaches are highlighted. One is statistical and uses data gathered from sections on different planes to generate a grain structure and then assign orientations to the individual grains. The second, more data-intensive approach is to perform serial sectioning and reconstruct the three-dimensional microstructure by optimizing the alignment or registration between adjacent layers. We present a new registration method that minimizes the crystallographic misorientation between layers, thus exploiting the orientation information inherent in the EBSD data sets.

3. The microstructural characteristics of a directly measured microstructure are compared with those of three-dimensional microstructures obtained from the statistical reconstruction method and from a three-dimensional Monte Carlo simulation of grain growth.

4. The analysis of the three-dimensional spatial distribution of second-phase particles whose alignment is important for the properties of the material is discussed. An example of such a distribution is presented for a structural aluminum alloy that contains a few percent by volume of intermetallic particles.

ACKNOWLEDGMENTS

LITERATURE CITED

1. Becker R, Panchanadeeswaran S. 1995. Effects of grain interactions on deformation and local texture in polycrystals. *Acta Metall. Mater.* 43:2701–19

2. Suresh S. 1998. *Fatigue of Materials*. Cambridge, UK: Cambridge Univ. Press. 617 pp.

3. Demirel MC, El-Dasher BS, Adams BL, Rollett AD. 2000. Studises on the accuracy of electron backscatter diffraction measurements. In *Electron Backscatter Diffraction In Materials Science*, ed. AJ Schwartz, M Kumar, BL Adams, pp. 65–74. New York: Kluwer Acad./Plenum

4. Wright SI. 1993. A review of automated orientation imaging microscopy (OIM). *J. Comp. Assist. Microsc.* 5:207–21

5. Matthies S, Wagner F. 1999. Using sets of individual orientations for ODF determination. *ICOTOM-12*, pp. 40–45. Montréal: NRC Res. Press

6. Costa LDF, Cesar RM, Cesar J. 2000. *Shape Analysis and Classification: Theory and Practice*. Boca Raton, FL: CRC Press. 660 pp.

7. Williams RE. 1968. Space-filling polyhedron: its relation to aggregates of soap bubbles, plant cells, and metal crystallites. *Science* 161:276–77

8. Torquato S. 2001. *Random Heterogeneous Materials: Microstructure and Macroscopic Properties*. New York: Springer Verlag. 218 pp.

9. Corson PB. 1974. Correlation functions for predicting properties of heterogeneous materials. I. Experimental measurement of spatial correlation functions in multiphase solids. *J. Appl. Phys.* 45:3159–64

10. Corson PB. 1974. Correlation functions for predicting properties of heterogeneous materials. III. Effective elastic moduli of two-phase solids. *J. Appl. Phys.* 45:3171–79

11. Corson PB. 1974. Correlation functions for predicting properties of heterogeneous materials. IV. Effective thermal conductivity of two-phase solids. *J. Appl. Phys.* 45:3180–82

12. Corson PB. 1974. Correlation functions for predicting properties of heterogeneous materials. II. Empirical construction of spatial correlation functions for two-phase solids. *J. Appl. Phys.* 45:3165–70

13. Adams BL, Morris PR, Wang TT, Willden KS, Wright SI. 1987. Description of orientation coherence in polycrystalline materials. *Acta Metall.* 35:2935–46

14. Lee PS, Piehler HR, Rollett AD, Adams BL. 2002. Texture clustering and long-range disorientation representation methods: application to 6022 aluminum sheet. *Metall. Mater. Trans. A* 33:3709–18

15. Kurtz S, Carpay F. 1980. Microstructure and normal grain growth in metals and ceramics. Part I. Theory. *J. Appl. Phys.* 51:5725–44

16. Kurtz S, Carpay F. 1980. Microstructure and normal grain growth in metals and ceramics. Part II. Experiment. *J. Appl. Phys.* 51:5745–54

17. Srolovitz DJ, Anderson MP, Sahni PS, Grest GS. 1984. Computer simulation of grain growth. II. Grain size distribution, topology and local dynamics. *Acta Metall.* 32:793–802

18. Bunge H. 1982. *Texture Analysis in Materials Science*. London: Butterworths. 593 pp.

19. Kocks UF, Tomé C, Wenk HR, eds. 1998. *Texture and Anisotropy*. Cambridge, UK: Cambridge Univ. Press. 675 pp.

20. Morawiec A. 2003. *Orientations and Rotations*. Berlin: Springer. 200 pp.

21. Randle V, Engler O. 2000. *Texture Analysis: Macrotexture, Microtexture & Orientation Mapping*. Amsterdam, Holland: Gordon & Breach. 388 pp.

22. Altmann SL. 1986. *Rotations, Quaternions and Double Groups*. Oxford, UK: Clarendon Press. 317 pp.

23. Takahashi Y, Miyazawa K, Mori M, Ishida Y. 1986. Quaternion representation of the orientation relationship and its application to grain boundary problems. *JIMIS-4*, pp. 345–52. Minakami, Japan: Trans. Japan Inst. Metals

24. Zhao JW, Adams BL. 1988. Definition of an asymmetric domain for intercrystalline misorientation in cubic materials in the space of Euler angles. *Acta Crystallogr. A* 44:326–36

25. Han TS, Dawson PR. 2005. Lattice strain partitioning in a two-phase alloy and its redistribution upon yielding. *Mater. Sci. Eng. A* 405:18–33

26. Saylor DM, Morawiec A, Rohrer GS. 2003. The distribution of grain boundaries in magnesia as a function of five macroscopic parameters. *Acta Mater.* 51:3663–74

27. Schaeben H, Apel M, Frank T, Iwanowski M, Zaefferer S. 2005. 3-Dimensional fabric reconstruction from 2-dimensional orientation images. *Mater. Sci. Forum* 495–497:185–90

28. Fernandes CP, Magnani FS, Philippi PC, Daian JF. 1996. Multiscale geometrical reconstruction of porous structures. *Phys. Rev. E* 54:1734–41

29. Oren PE, Bakke S. 2002. Process based reconstruction of sandstones and prediction of transport properties. *Transp. Porous Media* 46:311–43

30. Oren PE, Bakke S. 2003. Reconstruction of Berea sandstone and pore-scale modelling of wettability effects. *J. Petrol. Sci. Eng.* 39:177–99

31. Sundararaghavan V, Zabaras N. 2005. Classification and reconstruction of three-dimensional microstructures using support vector machines. *Comput. Mater. Sci.* 32:223–39

32. Talukdar MS, Torsaeter O. 2002. Reconstruction of chalk pore networks from 2D backscatter electron micrographs using a simulated annealing technique. *J. Petrol. Sci. Eng.* 33:265–82

33. Talukdar MS, Torsaeter O, Ioannidis MA. 2002. Stochastic reconstruction of particulate media from two-dimensional images. *J. Colloid Interf. Sci.* 248:419–28

34. Talukdar MS, Torsaeter O, Ioannidis MA, Howard JJ. 2002. Stochastic reconstruction of chalk from 2D images. *Transp. Porous Media* 48:101–23

35. Talukdar MS, Torsaeter O, Ioannidis MA, Howard JJ. 2002. Stochastic reconstruction, 3D characterization and network modeling of chalk. *J. Petrol. Sci. Eng.* 35:1–21

36. Basanta D, Miodownik MA, Holm EA, Bentley PJ. 2004. Evolving 3D microstructures using a genetic algorithm. *Mater. Sci. Forum* 467–470:1019–24

37. Basanta D, Miodownik MA, Holm EA, Bentley PJ. 2005. Using genetic algorithms to evolve three-dimensional microstructures from two-dimensional micrographs. *Metall. Mater. Transact. A* 36A:1643–52

38. Yi YB, Wang CW, Sastry AM. 2004. Two-dimensional vs. three-dimensional clustering and percolation in fields of overlapping ellipsoids. *J. Electrochem. Soc.* 151:A1292–300

39. Saylor DM, Fridy J, El-Dasher BS, Jung KY, Rollett AD. 2004. Statistically representative three-dimensional microstructures based on orthogonal observation sections. *Metall. Mater. Trans.* 35A:1969–79

40. Shimada K, Yamada A, Itoh T. 2000. Anisotropic triangulation of parametric surfaces via close packing of ellipsoids. *Int. J. Comp. Geom. Appl.* 10:417–40

41. Brahme A, Alvi MH, Saylor D, Fridy J, Rollett AD. 2006. 3D reconstruction of microstructure in a commercial purity aluminum. *Scripta Mater.* 55:75–80

42. Miodownik M, Godfrey A, Holm E, Hughes D. 1999. On boundary misorientation distribution functions and how to incorporate them into three-dimensional models of microstructural evolution. *Acta Mater.* 47:2661–68

43. Cahn JW, Fullman RL. 1956. On the use of lineal analysis for obtaining particle size distribution functions in opaque samples. *Transact. Am. Inst. Mining Metall. Eng.* 206:610–12

44. Saltykov SA. 1958. *Stereometric Metallography*. Moscow: Metallurgizdat

45. Underwood E. 1970. *Quantitative Stereology*. New York: Addison-Wesley. 274 pp.

46. Etinghof P, Adams BL. 1993. Representations of polycrystalline microstructure by *n*-point correlation tensors. *Text. Microstruct.* 21:17–37

47. Gacsi Z, Kovacs J, Pieczonka T. 2003. Particle arrangement characterization by the pair correlation function. *Powder Metall. Prog.* 3:30–38

48. Marthinsen K, Fridy JM, Rouns TN, Lippert KB, Nes E. 1998. Characterization of 3-D particle distributions and effects on recrystallization kinetics and microstructure. *Scripta Mater.* 39:1177–83

49. Rollett AD, Saylor DM, Fridy J, El-Dasher BS, Brahme A, et al. 2004. Modeling microstructures in 3D. *NUMIFORM 2004*, pp. 71–77. Columbus, OH: Am. Inst. Phys.

50. Tewari A, Gokhale AM, Spowart JE, Miracle DB. 2004. Quantitative characterization of spatial clustering in three-dimensional microstructures using two-point correlation functions. *Acta Mater.* 52:307–19

51. Tong WS, Rickman JM, Barmak K. 1999. Quantitative analysis of spatial distribution of nucleation sites: microstructural implications. *Acta Mater.* 47:435–45

52. Rintoul MD, Torquato S. 1997. Reconstruction of the structure of dispersions. *J. Colloid Interface Sci.* 186:467–76

53. Singh H, Gokhale AM, Mao Y, Spowart JE. 2006. Computer simulations of realistic microstructures of discontinuously reinforced aluminum alloy (DRA) composites. *Acta Mater.* 54:2131–43

54. Rollett AD, Campman R, Saylor D. 2006. Three dimensional microstructures: statistical analysis of second phase particles in AA7075-T651. *Mater. Sci. Forum* 519–521:1–10

55. Roberts CG, Semiatin SL, Rollett AD. 2006. Particle-associated misorientation distribution in a nickel-base superalloy. *Scripta Mater.* In press

56. Lee SB, Rickman JM, Rollett AD. 2007. Three-dimensional simulation of isotropic coarsening in liquid phase sintering. I. Model. *Acta Mater.* 55:615–26

57. Tikare V, Cawley JD. 1998. Numerical simulation of grain growth in liquid phase sintered materials. I. Model. *Acta Mater.* 46:1333–42

58. Tikare V, Cawley JD. 1998. Numerical simulation of grain growth in liquid phase sintered materials. II. Study of isotropic grain growth. *Acta Mater.* 46:1343–56

59. Rowenhorst DJ, Kuang JP, Thornton K, Voorhees PW. 2006. Three-dimensional analysis of particle coarsening in high volume fraction solid-liquid mixtures. *Acta Mater.* 54:2027–39

60. Morawiec A, Saylor D. 1999. Registry between sections in precision sectioning of polycrystalline materials. *ICOTOM-12*, pp. 198–203. Montréal, Ottawa: NRC Res. Press

61. Saylor DM, Morawiec A, Rohrer GS. 2002. The distribution and energies of grain boundaries as a function of five degrees of freedom. *J. Am. Ceram. Soc.* 85:3081–83

62. Saylor DM, El-Dasher BS, Adams BL, Rohrer GS. 2004. Measuring the five parameter grain boundary distribution from observations of planar sections. *Metall. Mater. Trans.* 35A:1981–89

63. Homer ER, Adams BL, Fullwood DT. 2006. Recovery of the grain boundary character distribution through oblique double-sectioning. *Scripta Mater.* 54:1017–21

64. Konrad J, Zaefferer S, Raabe D. 2006. Investigation of orientation gradients around a hard Laves particle in a warm-rolled Fe_3Al-based alloy using a 3D EBSD-FIB technique. *Acta Mater.* 54:1369–80

65. Lee SG, Gokhale AM, Sreeranganathan A. 2006. Reconstruction and visualization of complex 3D pore morphologies in a high-pressure die-cast magnesium alloy. *Mater. Sci. Eng. A* 427:92–98

66. Lewis AC, Bingert JF, Rowenhorst DJ, Gupta A, Geltmacher AB, Spanos G. 2006. Two- and three-dimensional microstructural characterization of a super-austenitic stainless steel. *Mater. Sci. Eng. A* 418:11–18

67. Lewis AC, Geltmacher AB. 2006. Image-based modeling of the response of experimental 3D microstructures to mechanical loading. *Scripta Mater.* 55:81–85

68. Lieberman SI, Gokhale AM, Tamirisakandala S. 2006. Reconstruction of three-dimensional microstructures of TiB phase in a powder metallurgy titanium alloy using montage serial sectioning. *Scripta Mater.* 55:63–68

69. Maruyama B, Spowart JE, Hooper DJ, Mullens HM, Druma AM, et al. 2006. A new technique for obtaining three-dimensional structures in pitch-based carbon foams. *Scripta Mater.* 54:1709–13

70. Rios PR, Dalpian TG, Brandao VS, Castro JA, Oliveira ACL. 2006. Comparison of analytical grain size distributions with three-dimensional computer simulations and experimental data. *Scripta Mater.* 54:1633–37

71. Rowenhorst DJ, Gupta A, Feng CR, Spanos G. 2006. 3D crystallographic and morphological analysis of coarse martensite: combining EBSD and serial sectioning. *Scripta Mater.* 55:11–16

72. Spowart JE. 2006. Automated serial sectioning for 3-D analysis of microstructures. *Scripta Mater.* 55:5–10

73. Uchic MD, Groeber MA, Dimiduk DM, Simmons JP. 2006. 3D microstructural characterization of nickel superalloys via serial-sectioning using a dual beam FIB-SEM. *Scripta Mater.* 55:23–28

74. Wahab AA, Hutchinson CR, Kral MV. 2006. A three-dimensional characterization of creep void formation in hydrogen reformer tubes. *Scripta Mater.* 55:69–73

75. Wu KM. 2005. 3-D morphology observation of degenerate ferrite in steel Fe-0.28C-3.0Mo using serial sectioning and computer-aided reconstruction. *Acta Metall. Sinica* 41:1237–42

76. Wu KM. 2006. Three-dimensional analysis of acicular ferrite in a low-carbon steel containing titanium. *Scripta Mater.* 54:569–74

77. Zaafarani N, Raabe D, Singh RN, Roters F, Zaefferer S. 2006. Three-dimensional investigation of the texture and microstructure below a nanoindent in a Cu single crystal using 3D EBSD and crystal plasticity finite element simulations. *Acta Mater.* 54:1863–76

78. Liu G, Yu H, Qin X. 2002. Three-dimensional grain topology–size relationships in a real metallic polycrystal compared with theoretical models. *Mater. Sci. Eng. A* 326:276–81

79. Schanuel S. 1986. What is the length of a potato? An introduction to geometric measure theory. *Springer Lect. Notes Math.* 1174:118–26

80. Rollett AD, Manohar P. 2004. The Monte Carlo method. In *Continuum Scale Simulation of Engineering Materials*, ed. D Raabe, F Roters, F Barlat, L-Q Chen, pp. 77–114. Weinheim, Ger.: Wiley-VCH

81. Lee PS, Piehler HR, Rollett AD, Adams BL. 2002. Texture clustering and long-range disorientation representation methods: application to 6022 aluminum sheet. *Metall. Trans. A* 33:3709–18

82. Dewobroto N, Bozzolo N, Barberis P, Wagner F. 2006. On the mechanisms governing the texture and microstructure evolution during static recrystallization and grain growth of low alloyed zirconium sheets (Zr702). *Int. J. Mater. Res.* 97:826–33